

# Energy potential of a tidal fence deployed near a coastal headland



# Energy Potential of a Tidal Fence Deployed Near a Coastal Headland

S. Draper[*1], A.G.L. Borthwick[†2], G.T. Houlsby[#3]

[*]*Centre for Offshore Foundation Systems, The University of Western Australia*
*Crawley, WA6009, Australia*
[1]Scott.Draper@uwa.edu.au

[†]*Department of Civil and Environmental Engineering, University College Cork*
*Cork, Ireland*
[2]a.borthwick@ucc.ie

[#]*Department of Engineering Science, University of Oxford*
*Parks Road, Oxford OX1 3PJ, U.K.*
[3]Guy.Houlsby@eng.ox.ac.uk

**Abstract**

Enhanced tidal streams close to coastal headlands appear to present ideal locations for the deployment of tidal energy devices. In this paper, the power potential of tidal streams near an idealised headland with a sloping seabed are investigated using a near-field approximation to represent a tidal fence, i.e. a row of tidal devices, in a 2D depth-averaged numerical model. Simulations indicate that power extracted by the tidal fence is limited because flow will bypass the fence, predominantly on the ocean side, as the thrust applied by the devices increases. For the dynamic conditions, fence placements and headland aspect ratios considered, the maximum power extracted at the fence is not related in any obvious way to local undisturbed kinetic flux or the natural rate of energy dissipation due to bed friction (although both of these have been used in the past as measures of the amount of power that may be extracted). The maximum extracted power is found to be insensitive to the size and spacing of devices within the fence; however the available power (equal to the extracted power net of vertical mixing losses in the immediate wake of devices) is optimized for devices with large area and small centre-to-centre spacing within the fence. The influence of energy extraction on the natural flow field is assessed relative to changes in the M2 component of elevation and velocity, residual bed shear stress and tidal dispersion.

**Keywords**— Tidal stream energy, tidal headland, tidal fence, actuator disc theory, shallow water equations

## 1. Introduction

A number of locations around the UK have been identified as promising sites for tidal stream energy extraction [1]. Interestingly, many of these locations can be described as enhanced tidal streams close to coastal headlands (e.g. Anglesey, Portland Bill, Mull of Kintyre, Dunscansby Head) and therefore have the important feature that the tidal streams are unbounded (on the ocean side) in the horizontal plane. This is in contrast to laterally bounded sites, such as tidal channels and narrow inlets to enclosed basins, which have been the focus of recent theoretical studies of tidal energy potential [2,3].

The deployment of tidal devices in a laterally unbounded flow is complicated by the fact that the removal of power may lead to flow diversion around the collection of devices, altering natural tidal streams and ultimately limiting power potential. Predicting this flow diversion is vital for accurate predictions of energy potential. However, despite this, previous energy resource assessments of headlands, e.g. [1], have usually been based on the undisturbed kinetic flux and do not appropriately account for the presence of devices or flow diversion. A notable exception is that due to Blunden and Bahaj [4,5] who conducted numerical simulations of an array of tidal devices, represented by an added bed roughness, close to the tip of Portland Bill, UK. The simulations highlighted that useful power extraction may be exploited from currents close to a headland (in this case, 60-70 MW). They also indicated that, with energy extraction, the magnitude and orientation of the M2 tidal currents in the vicinity of the array could change by approximately 15 % and up to $10^{o}$. However, although these simulations provide useful insight into the potential and effect of energy extraction close to an actual headland by explicitly including tidal devices, they are restricted to one specific turbine array location and a single level of added bed roughness. Consequently the results do not establish whether a limit to energy extraction exists for devices deployed near

to a headland. They also do not consider the effects of extraction on tidal dynamics not encapsulated by the M2 component.

A method to represent an ideal tidal fence in a 2D depth-averaged numerical model is described in [6]. A near-field approximation (extending multiple device diameters around the fence) is applied to the flow through a line of actuator discs, with known porosity and diameter, to define a tidal fence as a line sink of momentum in a far-field tidal flow (encompassing the coastal region). The method has the advantage that it allows a direct link to be made between the actual geometry of a fence of ideal devices and the momentum sink the devices impart in a tidal stream. More importantly, the near-field solution defines the efficiency of the tidal fence, which determines the fraction of extracted power removed by the fence that is available to devices within the fence after subtracting unavoidable vertical mixing losses in their immediate wake.

The present paper uses the method in [6] to introduce a tidal fence near to an idealised headland. A brief review of [6] is given in Section 2 and the idealised headland is introduced in Section 3. Sections 4 and 5 analyse the extracted power and available power, together with the effects of energy extraction on the local flow field.

## 2. Simulating a Tidal Fence

### (a) Near-Field Approximation

An extension of the classic actuator disc analysis, used in wind turbine design, is described in [6] that accounts for gravity, finite volume effects associated with the free surface, and

downstream mixing. The analysis leads to an expression for the depth perturbation across a fence given functionally by

$$\Phi = \frac{\Delta h}{h} = \frac{h - h_5}{h} = \Phi\left(F_r = \frac{U}{\sqrt{gh}}, B = \frac{A}{bh}, \alpha_2\right), \tag{1}$$

where $h$ and $h_5$ define the water depths immediately upstream and downstream of the fence (see figure 1), $F_r$ is the Froude number immediately upstream of the fence defined in terms of the depth-averaged velocity component $U$ normal to the fence, $B$ is the blockage ratio of a device of area $A$ deployed with centre-to-centre spacing $b$ within the fence, and $\alpha_2$ defines the velocity $\alpha_2 U$ passing through the devices and thus their porosity. In general $B$ and $\alpha_2$ can vary slowly along the fence. It is also possible to specify a wake velocity coefficient $\alpha_4$, defining the velocity $\alpha_4 U$ in the wake of the devices, in place of $\alpha_2$. In that case $\alpha_2$ is then an implicit function of $F_r$, $B$ and $\alpha_4$ and is greater than, but varies monotonically with, $\alpha_4$ (see [6]).

The depth change in (1) is caused by the thrust applied by the fence, $T = C_{\mathrm{d,eff}} \rho u^2 bh$, where $C_{\mathrm{d,eff}}$ is an effective depth-averaged thrust coefficient that can vary with the Froude number and is defined by [6]

$$\frac{\Phi^3}{2} - \frac{3\Phi^2}{2} + \left(1 - F_r^2\left(1 - C_{\mathrm{d,eff}}\right)\right)\Phi - F_r^2 C_{\mathrm{d,eff}} = 0. \tag{2}$$

Intuitively, for a fixed $B$ the depth-averaged thrust coefficient increases as the turbines become less porous (i.e. when $\alpha_2$ or $\alpha_4$ reduces), whereas for fixed $\alpha_2$ or $\alpha_4$, $C_{\mathrm{d,eff}}$ increases with blockage $B$.

The power extracted by the fence, including any mixing losses in the immediate wake of the devices (i.e. over the length $l_v$ in figure 1), is

$$P = \rho g U_* \Phi h^2 \left(1 - Fr^2 \frac{1 - \Phi/2}{(1-\Phi)^2}\right), \tag{3}$$

and the fraction of the extracted power not lost in mixing immediately behind the fence, and therefore available to the devices, is given by the efficiency

$$\eta \cong \alpha_2 \left(1 - \frac{\Delta h}{2h}\right). \tag{4}$$

Thus, provided $F_r$ is obtained from an appropriate far-field solution the local depth change across a fence, with known B and $\alpha_4$, can be calculated by (1) and the efficiency by (4).

It should be noted that the near field approximation is theoretically valid within an infinitely long fence of periodically placed devices. It is, however, used here as a first approximation at all positions along a fence of finite length.

### (b) Far-Field Approximation

The far-field tidal flow is simulated by solving the depth-averaged shallow water equations using the Discontinuous Galerkin (DG) Finite Element Method [7]. The perturbation in depth defined by (1) is introduced as a line sink of momentum by altering the numerical flux between elements surrounding the fence (see [6,7] for more detail). However, to avoid the development of a velocity singularity at the ends of the turbine fence in a laterally unbounded flow, the scheme adopted here replaces (1) (Eq. 19d in [6]) with

$$\frac{\Delta h}{h} = \gamma \times \Phi(F_r, B, \alpha_2), \tag{5}$$

in which,

$$\gamma = \begin{cases} -2\left(\frac{|x'|}{\delta L_f}\right)^3 + 3\left(\frac{|x'|}{\delta L_f}\right)^2, & |x'| < \delta L_f \\ 1, & |x'| \geq \delta L_f \end{cases},$$

where $x'$ is the shortest distance from …. to the edge of the fence, $L_f$ is the length of the fence and $\delta$ is a constant that defines a smoothing in the momentum sink at the edge of the fence. In the simulations to follow, a value of $\delta = 1/40$ has been adopted throughout.

It should be noted that the results presented in this paper do not depend on the manner in which the line sink of momentum is introduced numerically; similar results are obtained using a sufficiently thin strip of added bed roughness given by $k = C_{d,eff}h/T$, where $T$ is the thickness of the strip.

## 3. Idealised Tidal Headland

To investigate energy extraction near to a coastal headland, an idealised coastline, similar to that considered by [8], is adopted as illustrated in figure 2. The headland shape approximates the function $L_1 \exp[-(5x/L_2)^2/2]$, where $x$ is …., $L_1$ is the offshore extent and $L_2$ is the breadth at a distance ~$0.96L_1$ from the tip of the headland. Following [8] and [9] a sloping bathymetry is used to create the coastal boundary layer flow, instead of specifying a vertical no-slip boundary condition. The headland is located in a channel of width $W$ to represent the coastline typical of many UK sites (e.g. the Mull of Kintyre located within the Northern Passage to the Irish Sea). Boundary conditions comprise: a clamped sinusoidal current $U_0 \sin(\omega t)$ at the west upstream boundary; a non-reflecting radiation condition at the east downstream boundary; and no-slip reflective walls along the south and north coastlines (which become slip walls when $\upsilon_T = 0$ m$^2$/s). Isoparametric elements are used along the headland tip to ensure that flow separation is not mesh dependent. High-order quartic basis functions are used in the DG solution to resolve the transient features close to the headland.

Following [8] the tidal dynamics near to the headland are varied by altering the dimensionless numbers (i) Aspect ratio $\phi = 2L_1/L_2$; (ii) Effective drag ratio $C_d' = C_d L_2/(2h_0)$; and (iii) Keulegan-Carpenter number $K_c = 2U_0/(\omega L_2)$. In these numbers $C_d$ is a constant bed friction coefficient, $h_0$ is the offshore still water depth, $U_0$ is the alongshore depth-averaged velocity magnitude far from the headland, and $\omega$ is the tidal angular frequency. For a given aspect ratio it is shown in [8] that the importance of friction to advection and advection to acceleration in the momentum balance, which are defined respectively by $C_d'$ and $K_c$, indicate whether separation will result at the headland tip and, if separation does occur, the evolution of the resulting eddies in the local flow field. In general separation is more likely when the coastline is deep, the headland length scales are small relative to the tidal wavelength and the seabed is smooth (i.e. $1/C_d' \gg 1$ or $K_c \gg 1$). It is also more likely when the headland has a narrow aspect ratio ($\phi \gg 1$).

Four headland cases are considered here (Table1). The dimensionless ratios span a similar range to UK headlands [7]. In all cases: $\omega = 0.00014$ rad/s, $U_0 = 1.5$ m/s, $h_0 = 30$ m, $f = 0$ rad/s and $\upsilon_T = 0$ m$^2$/s. (The effects of Coriolis acceleration and eddy viscosity are discussed in Section 6.)

### (a) Natural Tidal Flow

In the natural state without energy extraction, the water elevation field around the headland in Case 1 (a rough approximation to tidal flow around Anglesey) can be described in terms of M2 elevation co-amplitude lines as shown in figure 3(a). These lines converge towards the headland tip where the acceleration of the flow around the headland is largest. The elevation co-tidal lines (not shown) converge near the headland tip, as predicted in [10]. Figure 3(a) also shows the tidal velocity field at the time of maximum tidal current ($t/T = 1/4$). Enhanced currents are evident close to the headland tip. However, since the velocity reduces

towards the coastline where the frictional force per unit depth is largest, the location of maximum velocity (~3.3 m/s or roughly twice the background velocity) is located ~5 km from the headland tip. To illustrate the importance of the basic dynamic conditions on the natural tidal flow, figures 3(b) and (c) show the instantaneous velocity field close to maximum tidal current $(t/T = 1/4)$ for Cases 2 and 3. Transient eddies advecting far from the headland tip are most pronounced for Case 3, which has a similar dynamic balance to Portland Bill. In contrast, the flow field for Case 2 has no identifiable transient features, indicating that the flow has not separated and is in agreement with [8].

### (b) Previous Metrics of Energy Extraction

Undisturbed kinetic flux has previously been used as a basis to determine the tidal resource in the UK [1]. A slightly different metric, defined as the power density,

$$P_d = \frac{1}{2}\rho\overline{|\boldsymbol{u}|^3}, \tag{6}$$

where the overbar denotes averaging over a tidal cycle, is displayed in the Atlas of UK Marine Renewable Energy [11].

The integral of this quantity over a plan area is proportional to the natural power dissipation and is also sometimes used to imply the tidal resource. For reference, figure 4 plots the kinetic flux for Case 1. It is evident that the headland creates a region of elevated kinetic flux, which, because of the sloping seabed and higher frictional force per unit depth at the coastline, moves the location of maximum kinetic flux some distance offshore. Furthermore the region of high flux does not coincide with the region where transient eddies are formed in the wake of the headland. The power density (not shown) is more representative of the depth-averaged velocity and has a maximum slightly closer to the headland tip.

## 4. Power Potential

The flow field at the point of maximum tidal current ($t/T \sim 1/4$) is shown in figure 5 for Case 1 when a tidal fence is deployed in the location of highest natural flux (see figure 2 for location). In each simulation considered, the devices within the fence have $\alpha_4 = 1/3$ and a different fixed blockage ratio. It is evident that the instantaneous velocity through the fence reduces with increasing blockage ratio. This trade-off between blockage ratio (or effective resistance of the fence) and the local velocity through the fence is qualitatively similar to that between porosity and velocity in the classic Lanchester-Betz actuator disc analysis. For the tidal fence, no power can be extracted at either of the two extremes of zero or unit blockage ratio; power extraction is maximum at some intermediate (optimum) blockage ratio. A similar result should apply for any fence deployed in a laterally unbounded flow.

The extracted power, averaged over a tidal cycle, is plotted in figure 6(a) as a function of the maximum total flow rate through the fence, $Q_f$ for several blockage ratios. Up to 560 MW can be extracted when $Q_f \approx 60\%$ of the maximum in the natural state and the blockage ratio is close to 0.6. Given that $\alpha_4 = 1/3$, the overall efficiency of the devices within the fence is approximately 41 % over the tidal cycle, implying that only 230 MW is available for generation.

There is little variation in power extraction over the length of the fence (not shown). However, prior to maximum extraction slightly more power (between 1 and 15%) is removed from the southern end of the fence. Beyond maximum power extraction, an increasing proportion of the power comes from the northern end of the fence. Although not pursued here, the model could be used to optimise the distribution of devices along the fence.

To compare the extracted power with natural energy dissipation figure 6(a) displays the total power dissipated (due to bed friction and the turbine fence) in a reference area surrounding the fence (see figure 2). It is evident that the total dissipation also has a maximum value, which peaks before [should this be after???] that of the turbine fence itself. The difference between both curves, which represents the power that is dissipated naturally due to bed friction, decreases monotonically with the fence blockage ratio. The undisturbed time-averaged kinetic flux passing through the location of the turbine fence (also illustrated in figure 6(a)) overestimates the maximum power extraction.

**(a) Variation in Dynamic Balance**

Figures 6(b) and (c) present the extracted power curves for Cases 2 and 3, together with the undisturbed kinetic flux and natural power dissipation. For Case 2 the natural dissipation is higher than the maximum extracted power, whilst for Case 3 the natural dissipation is significantly lower. This suggests, independent of the reference area selected, that natural dissipation does not provide a useful guide to power potential over a realistic range of tidal dynamics. The result is perhaps to be expected, given that a fence deployed near to a headland with no seabed drag could still extract energy but, of course, the natural dissipation would be zero and provide no guide to the maximum energy extraction.

A lack of universal correlation between the undisturbed time-averaged kinetic flux and the maximum extracted power is illustrated by the different headland cases in figure 6, with the ratio of extracted power to undisturbed kinetic flux equal to approximately 1.2, 1.6 and 0.7 for Cases 1, 2 and 3, respectively. The highest kinetic efficiency (defined as the optimal power potential divided by the kinetic flux) is achieved for Case 2, where friction forces are the largest compared to advection (i.e. largest $C_d'$) and local acceleration is the largest compared with advection (i.e. smallest $K_c$). This suggests that it is harder for flow to bypass a

fence when the seabed friction and local acceleration surrounding the fence are significant, compared with advection, in the natural state. More importantly the results in figure 6 indicate that the undisturbed time-average kinetic flux appears to be a poor predictor of the energy potential in the vicinity of a tidal headland because it cannot explain the ability of the flow to divert around the turbine fence. (It should be noted that this is different to the discussion in [2,3], where the natural kinetic flux was seen to be a poor indicator of the energy potential for a tidal channel because the flow rate through the channel, and consequently the kinetic flux, reduced with energy extraction.)

Comparing the absolute maximum power extraction across all three cases most power is extracted in Case 1, followed by Case 2 (530 MW) and Case 3 (50 MW). Consequently in these simulations, although Case 2 has higher kinetic efficiency than Case 1, Case 2 extracts less power than Case 1 because, for the fixed western boundary tidal current, the increased bed friction in Case 2 reduces natural tidal currents and kinetic flux at the headland tip. The extracted power in Case 3 is 9% of that in Case 1 because the turbine fence deployed in Case 3 has reduced cross-sectional area (approx. 15% of Case 1) and because it is relatively easier for the flow to bypass, consistent with the kinetic efficiency.

### (b) Location of Turbine Fence

Despite the inability of natural kinetic flux to determine absolute power extraction, it is nevertheless intuitive that the location of maximum kinetic flux may indicate the best position to site tidal devices. For example figure 7(a) shows the power extracted at two alternative fence locations. In both cases, it is evident that placing the turbine fence away from the location of maximum natural kinetic flux results in significantly less power, even though placing the turbine fence further offshore results in more power than moving the fence

closer to the coastline. The kinetic efficiency of the fence is 1.7 and 0.8 for Positions 1 and 2, respectively, compared with 1.2 for Case 1. As the turbine is placed further offshore the extracted power is therefore a higher fraction of the undisturbed flux. This indicates that the flow bypasses the fence most easily when it is placed in shallow water next to the headland, and is consistent with the surrounding water on the ocean side being relatively deeper so as to offer less impedance to the bypassing flow.

### (c) Variation in Geometry

To examine what effect the headland shape has on the flow field figure 7(b) plots the undisturbed kinetic flux for Cases 1 and 4. The power extracted by the fence of turbines declines substantially as the aspect ratio $\phi$ reduces. This is despite the fact that the channel width, measured between the tip of the headland and the northern channel wall ($W - L_1$), is identical for both aspect ratios. Consequently the shape of the headland can have a significant effect on the power potential, for a given background tidal current.

### (d) Available Power

It was noted in [6] that operating at a wake velocity coefficient higher than $1/3$ can increase device efficiency by reducing mixing losses. Figure 8(a) therefore plots the extracted power for Case 1 as a function of the fence depth-averaged turbine thrust $C_{\mathrm{d,eff}}$ (computed when $F_r = 0$) for fences of devices with various fixed $\alpha_4$ values. Interestingly, although the near-field solution indicates that for each fence the depth-averaged turbine thrust coefficient $C_{\mathrm{d,eff}}$ will vary over the tidal cycle with Froude number by an amount dependent on the depth change (Eq. (2)) and therefore the particular fence blockage ratio and wake velocity coefficient (Eq. (1)), all points appear to lie on the same line in figure 8(a), with only minor

deviation for $\alpha_4 = 3/4$ at higher $C_{\mathrm{d,eff}}$ values. This result suggests that for realistic blockage ratio and wake velocity coefficient the variation in $C_{\mathrm{d,eff}}$ with $F_r$ over the tidal cycle, which should be different for different fences, must have a negligible effect on power extraction. The coefficient $C_{\mathrm{d,eff}}$ calculated for $F_r = 0$ therefore uniquely defines the power extraction to good approximation. A similar result was also observed for Cases 2, 3 and 4 (not shown).

Exploiting the weak dependence of $C_{\mathrm{d,eff}}$ on $F_r$ the extracted power can be calculated for a fence of any given $B$ and $\alpha_4$ by first computing $C_{\mathrm{d,eff}}$ with $F_r = 0$ and then interpolating the extracted power from the curve in figure 8(a). The available power can then be found to an acceptable level of accuracy by multiplying the extracted power by the efficiency in (4) assuming $F_r = 0$. Using this approach the extracted power and available power, normalised by the maximum extractable power, are plotted for Cases 1 and 3 as a function of fence blockage ratio and wake velocity coefficient in figures 8(b) and (c). Consistent with the findings in [12], figure 8(b) shows that maximum power extraction can be achieved for a range of combinations of $\alpha_4$ and $B$ (dashed lines), with each combination having the same (optimal) coefficient $C_{\mathrm{d,eff}}$ highlighted in figure 8(a). The fraction of maximum power available to the devices within the fence, however, is maximised when the blockage ratio and wake velocity coefficient approach unity (figure 8(c)). This is because devices with large $B$ and $\alpha_4$ are most efficient [6] and provide sufficient thrust to extract the maximum power.

Interestingly, for general blockage ratio (i.e. $B = 0.5$ in figure 8) the available power is maximised when power extraction is not maximised (see the solid circles in figure 8). This is because the gain in efficiency achieved by operating at a higher $\alpha_4$ than required for maximum extraction more than offsets the reduction in power extraction. Consequently, for typical values of $B$, the maximum available power may not coincide with the maximum

extracted power. Consistent with findings in [12] for a tidal channel, there is therefore a need to "tune" the velocity coefficient of a fence of devices near a headland to maximise available power. This tuning requires knowledge of the complete power curve in figure 8(a). For complicated coastal geometries such as headlands this curve can only be obtained using a model similar to that employed here.

Comparing the two cases in figure 8(c), it is interesting to note that a larger fraction of the maximum extractable power for a given fence blockage ratio below unity is available to the fence in Case 3 than Case 1 (see solid circles in figure 8), although more power in absolute terms is available for Case 1. This result is consistent with the requirement for the turbine fence in Case 1 to provide a higher effective thrust coefficient at maximum power, and at a given fraction thereof, to compete with the increased importance of bed friction and acceleration in the momentum balance (i.e. higher $C_d'$ and lower $K_c$). Since a higher thrust coefficient for a given blockage ratio can only be achieved with a lower velocity coefficient, the fence efficiency must reduce due to (3). This ultimately reduces the fraction of extractable power available to the devices for Case 1 at a given blockage ratio. It should also be noted that this result is true for all $B$ regardless of the fact that at suboptimal conditions of high $B$ and very low $\alpha_4$ (bottom right corner of figure 8(c)) the normalised extracted power, and consequently the normalised available power, is higher for Case 1.

Lastly figure 8(d) plots the available power at two locations along the fence for Case 1: one-fifth the distance from the northern and southern ends of the fence, respectively. For a given blockage ratio, it is evident that a higher fraction of the extracted power is available on the southern side of the fence. Since an identical blockage ratio and a very similar efficiency is

realised on both sides of the fence, this result is consistent with the slightly greater extraction of power noted on the southern side of the fence.

## 5. Effect on Natural Flow Conditions

For brevity, the analysis presented here is solely for Case 1. The results are qualitatively similar for the other cases.

### (a) M2 Tidal Constituents

For time-varying tidal currents, tidal ellipses are typically used to describe the flow field ([5] and [13]). Figure 9(a) displays the M2 tidal current ellipse minor and major axes at various points in the flow field for Case 1 without a turbine fence. Amplification of the major axis is obvious close to the headland tip, whereas the minor axis is generally small relative to the major axis for this particular headland case. Figure 9(b) presents changes to the ellipse parameters following the introduction of a turbine fence operating close to maximum energy extraction. It is evident that there is a reduction of the major axis immediately upstream and downstream of the fence, while an inclination (declination) in orientation of the ellipse, with reference to the positive $x$ axis, is evident further east (west) of the fence. This suggests that the flow tends to bypass on the ocean side. Moreover the reduction in the time-averaged absolute total flow rate through the fence is $8.2\times 10^{4}$ $m^3/s$ at maximum extraction, whereas the increase in time-averaged absolute total flow rate passing between the fence and coastline is just $7.6\times 10^{3}$ $m^3/s$. In the presence of energy extraction, the M2 elevation co-amplitude and co-tidal lines (not shown) concentrate towards the end of the turbine fence, consistent with the accelerating flow around the fence. An effect similar to this was noted by [5] for energy extraction close to Portland Bill.

The substantial change in the velocity field implied by figure 10(b) indicates that the addition of a tidal device may have a significant impact on the local environment. As a compromise it is interesting to consider energy extraction at, say, one half of the maximum power extraction. In this case, simulations show the maximum flow rate through the fence decreases by 17% as opposed to 44 % incurred at maximum power. This implies that a fraction of the maximum power can be removed in the vicinity of the headland for a comparatively smaller fractional change in the natural flow conditions, and is entirely consistent with the power curves presented in figure 6.

### (b) Mean Stress and Tidal Dispersion

Although the M2 constituents provide some insight into the effects of energy extraction on natural hydrodynamics, the local flow field is inherently nonlinear [8,9]. This non-linearity gives rise to compound and residual tides and contributes to residual bed shear stress and tidal dispersion. The addition of tidal devices can have an impact on these non-linear quantities.

The importance of the residual shear stress on sand transport has been demonstrated in a study of the Southern UK [14], where the mean stress on the seabed was given by

$$\left(\overline{\tau_x}, \overline{\tau_y}\right) = \rho C_d \overline{\boldsymbol{u}|\boldsymbol{u}|} \,. \tag{7}$$

with $\boldsymbol{u}$ the depth-averaged velocity vector. Figure 10(a) plots this vector quantity for the headland in Case 1. Without energy extraction a slight asymmetry in the stress about the headland tip is evident, and is consistent with the propagation, from the west, of the damped progressive tidal wave. The general pattern of bottom stress is very similar to that calculated for actual headland sites [9] and is indicative of the continual scouring and deposition that leads to the observed grading of the seabed. To investigate the impact of energy extraction, figure 10(b) plots the vector difference in mean stress between natural conditions and those at

maximum power extraction. The obvious features are the four circular regions surrounding the ends of the turbine fence. Interestingly these residual stresses mimic the stress field at the tip of the headland suggesting that the tidal fence has a similar effect to that of an offshore island. The resulting changes to the bed shear stress could have a significant effect on bed load transport and grading at a sandy site, such as Portland Bill.

In addition to the changes to mean stress, an interesting finding illustrated in figure 9 is that the introduction of energy extraction in the vicinity of a headland augments natural tidal currents surrounding the turbine fence. This is in contrast to the placement of a turbine fence across a significant fraction of a narrow channel where, due to back effects on the flow rate through the channel, the velocity field close to the turbines may vary spatially but will generally be everywhere reduced.

The large spatial gradient in velocity between the flow passing through and bypassing the fence is expected to alter tidal dispersion in the vicinity of the headland. To investigate this further, Signell [15] suggests that a diffusion coefficient $K$ can be used to quantify the dispersion, or the degree of possible mixing, in a time-varying tidal flow. This coefficient can be related to the variance in position of a number of released particles or floats according to the expression

$$K = \frac{1}{2}\frac{d\sigma^2}{dt}, \tag{8}$$

where $\sigma^2$ is the spatial variance in the distribution of particles, with time $t$, relative to the time-varying mean position $(\overline{x},\overline{y})$. To obtain an estimate of this variance a box of $N$ regularly distributed particles can be introduced at a given location and tracked over a tidal cycle, giving a measure for $K$, assigned to the initial location, of [16]

$$K \approx \frac{1}{2}\left(\frac{\sigma_x^2(t+T)-\sigma_x^2(t)}{2T}+\frac{\sigma_y^2(t+T)-\sigma_y^2(t)}{2T}\right), \tag{9}$$

with $\sigma_x^2$ and $\sigma_y^2$ the variance in $x$ and $y$ positions of the $N$ particles relative to the time-varying mean position.

A useful location to investigate tidal dispersion is in the gap between the tidal fence and the coastline. Figure 11 presents snapshots of 153 particles released in a region $(x,y) \in [-1000,1000]\text{m} \times [4000,5000]\text{m}$ for Case 1 both with and without energy extraction. In the second of these plots, $t/T = 1$, the particles released with energy extraction are already beginning to stretch over a larger distance than those released without energy extraction due to the increased bypass velocity. At $t/T = 5$ many particles released in the presence of energy extraction have encountered the tidal fence (red particles) and there is a visible increase in dispersion compared to those particles released without energy extraction. The variation in $K$ over several tidal cycles is plotted for both scenarios in figure 12. The results confirm that tidal dispersion does increase when energy is extracted and implies that the mixing of suspended sediment and pollutant transport can be augmented (in this case by a factor of 2) close to the headland.

## 6. Discussion and Conclusions

In each of the simulations performed in this paper both Coriolis and viscous terms have been neglected. It is however easy to include both of these parameters in the numerical model. Setting the Coriolis parameter to $f = 0.00012$ rad/s (representative of latitude 55° North) and repeating the simulations for Case 1 led to an increase in maximum power extraction of ~20 %. This increase is to be expected since the effect of the Coriolis forcing on the eastward propagating tidal wave is to increase the tidal range and tidal currents close to the headland, which lie to the right hand side of the progressive wave. Introduction of depth-

averaged eddy viscosity coefficients of 1 $m^2/s$ and 5 $m^2/s$ had negligible effect on the extracted power (less than 5 % change) for all of the cases.

A main conclusion of this paper is that the power that can be extracted from a tidal fence located next to a tidal headland is limited because the flow can bypass the fence when energy is extracted. A detailed analysis of the flow field shows that the bypass flow is not symmetric around the fence, but is greater on the ocean side where the depth is greater. Importantly, natural dissipation and kinetic flux are not a consistent fraction of the maximum power extraction over the range in dynamic conditions typical of tidal headlands found around the UK. Despite this, the kinetic flux does appear to be potentially useful in identifying the best location to deploy a fence in the vicinity of a headland. It is not unreasonable to expect that this will also be the case for other laterally unbounded tidal flows.

Numerous combinations of device blockage ratio and velocity coefficient can be chosen to maximise fence power extraction. However, consistent with results discussed in [12] for a tidal channel, the available power is maximised when tidal devices with large blockage ratio and velocity coefficient are used within the fence. The results also demonstrate that the fraction of maximum extractable power available to devices within the fence is dependent on their location along the fence as well as the tidal dynamics. Moreover, a greater fraction of extractable power appears to be available, for a given blockage ratio, when acceleration and bed friction effects are small relative to advection terms in the momentum balance. However the maximum extracted power is largest in the opposite situation, when the acceleration and bed friction are larger relative to advection terms in the momentum balance.

Analysis of residual shear stress and tidal dispersion has indicated that energy extraction can augment both shear stress at the seabed and the potential for mixing of suspended material at a coastal headland site. Interestingly, the second of these may have beneficial environmental effects. For example energy extraction may improve the dilution of contaminants introduced at sewage outfalls, which are commonly located close to coastal headlands.

**Acknowledgments**

S.D. would like to thank Richard Soulsby for valuable discussions. Support from the Rhodes Trust, St Catherine's College, Oxford and the The Lloyd's Register Educational Trust is kindly acknowledged.

## References


[1] Black & Veatch Ltd. Phase II: UK Tidal Stream Energy Assessment. Technical Report, 2005.

[2] C. Garrett, and P. Cummins, "The power potential of tidal currents in channels", *Proc. R. Soc. Lond. A*, vol. 461, pp. 2563-2572, 2005.

[3] J. Blanchfield, C. Garrett, P. Wild, and A. Rowe, "The extractable power from a channel linking a bay to the open ocean," *Proc. IMechE Part A: J. Power Energy,* vol. 222, pp. 289–297, 2008.

[4] L.S. Blunden, and A.S. Bahaj, "Initial evaluation of tidal stream energy resources at the Portland Bill, UK," *Renew. Energy*, vol. 31, pp. 121-132, 2006.

[5] L.S. Blunden, and A.S. Bahaj, "Effects of tidal energy extraction at Portland Bill, Southern UK predicted from a numerical model," *Proc. Seventh EWTEC*, Porto, Portugal, 2008.

[6] S. Draper, G.T. Houlsby, M.L.G. Oldfield, and A.G.L. Borthwick, "Modelling tidal energy extraction in a depth-averaged coastal domain," *IET Renewable Power Generation*, vol. 4, Iss. 6, pp. 545-554, 2010.

[7] S. Draper "Tidal stream energy extraction in coastal basins", DPhil Thesis, University of Oxford, U.K., 2011.

[8] R.P. Signell, and W.R. Geyer, "Transient eddy formation around headlands," J. Geophysical Research, vol. 96, pp.2561-2575, 1991.

[9] R.D. Pingree, and L. Maddock, "The tidal physics of headland flows and offshore tidal bank formation," *Marine Geology*, vol. 32, pp. 269-289, 1979.

[10] G. I. Taylor, "Tidal friction in the Irish Sea," *Phil. Trans. Royal Society of London, Series A*, vol. 220, pp. 1-33, 1920.

[11] ABPmer, MET, Garrad Hassan, and Proudman Oceanographic Laboratory, "Atlas of UK Marine Renewable Energy Resources," 2004.

[12] R. Vennell, "Tuning turbines in a tidal channel," *J. Fluid Mechanics*, vol. 663, pp. 253-267, 2010.

[13] L. Maddock, and R.D. Pingree, "Numerical Simulation of the Portland Tidal Eddies," *Estuarine and Coastal Marine Science*, vol. 6, pp. 353-363, 1978.

[14] R.D. Pingree, and D.K. Griffiths, "Sand transport paths around the British Isles resulting from M2 and M4 tidal interactions", *Journal Marine Biology Ass.*, vol. 59, pp.497-513, 1979.

[15] R.P. Signell, "Tidal dynamics and dispersion around coastal headlands". PhD Thesis, Massachusetts Institute of Technology, USA, 1989.

[16] T. Awaji, N. Imasato, and H. Kunishi, "Tidal exchange through a strait: A numerical experiment using a simple model basin," *Journal of Physical Oceanography*, vol. 10, pp. 1499-1508, 1980.

## Tables and Captions

**Table 1:** Parameters used in idealised headland simulations.

| Case | Physical Parameters | | | Dimensionless Ratios | | |
|---|---|---|---|---|---|---|
| | $C_d$ | $L_1$ | $W$ | $\phi$ | $K_c$ | $1/C'_d$ |
| 1 | 0.0025 | 10 km | 50 km | 2.0 | 2.1 | 2.4 |
| 2 | 0.0050 | 10 km | 50 km | 2.0 | 2.1 | 1.2 |
| 3 | 0.0025 | 1 km | 7.5 km | 2.0 | 21 | 24 |
| 4 | 0.0025 | 10 km | 50 km | 1.0 | 1.05 | 1.2 |

## Figures and Captions

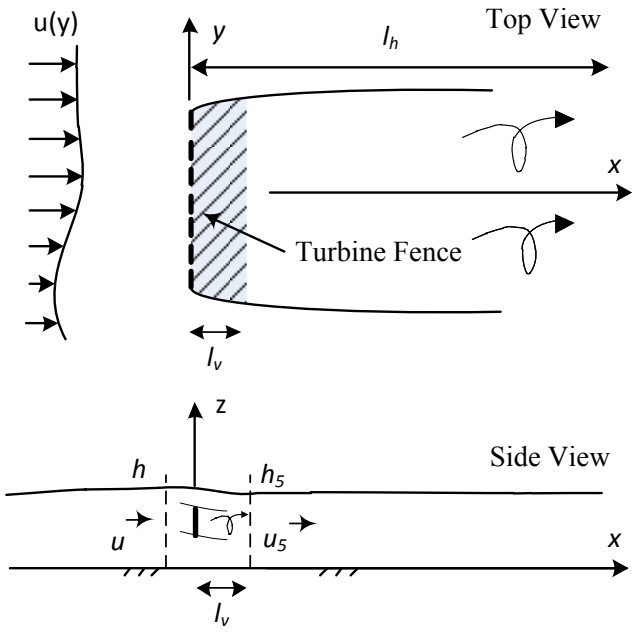


**Figure 1:** Turbine fence in depth-averaged flow, after [6]. A line momentum sink is a good representation when the vertical mixing length $l_v$ is much smaller than the fence length, the lateral mixing length $l_h$ and the numerical mesh size.

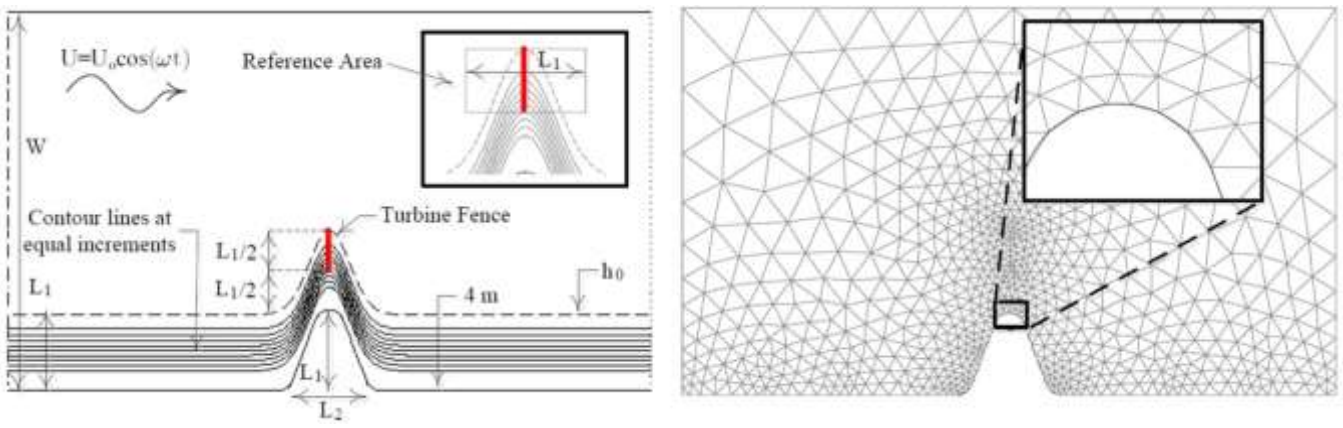


**Figure 2:** Domain and numerical mesh of idealised headland geometry, after [8]. Dashed contour line indicates extent of sloping bathymetry.

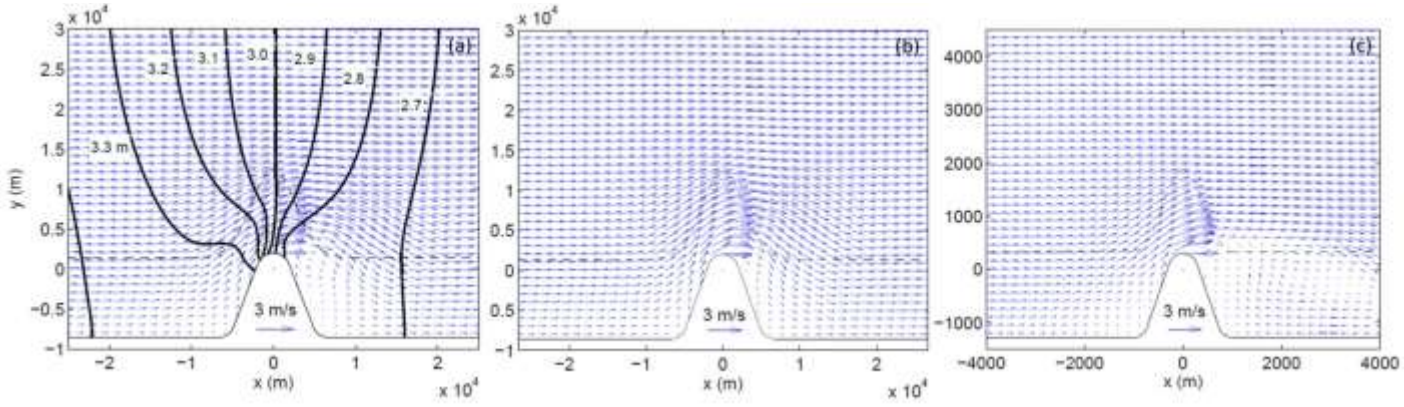


**Figure 3:** (a)-(c) Velocity vectors at $t/T = 1/4$ for Cases 1, 2 and 3, respectively. M2 co-amplitude lines are superimposed in (a) for Case 1.

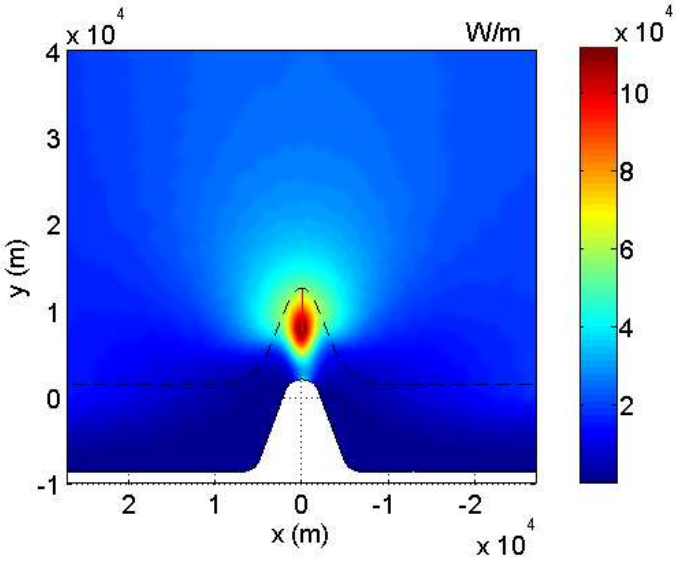


**Figure 4:** Kinetic flux (defined as $(1/2)\rho|u|^3h$ per meter width in the $y$ direction) averaged over a tidal period for Case 1 in the natural state.

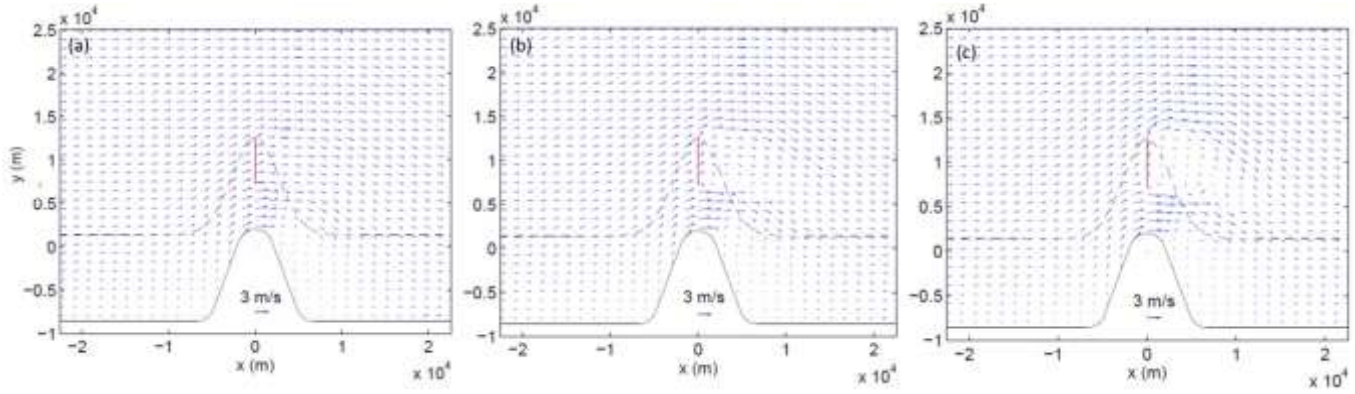


**Figure 5:** Velocity vectors at $t/T = 1/4$ for Case 1 with a tidal fence (red line) having blockage (a) $B = 0.4$, (b) $B = 0.6$, (c) $B = 0.8$.

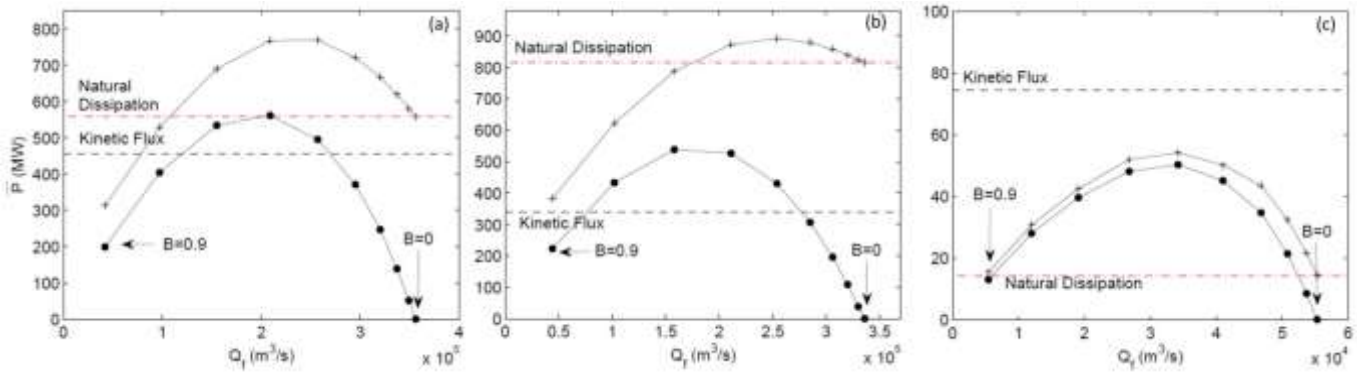


**Figure 6:** Average power extracted $\overline{P}$ by the fence $(-\bullet-)$ and total power dissipated in the reference area $(-+-)$ plotted as a function of the maximum flow rate through the fence $Q_f$. (a)-(c) Cases 1-3, respectively. Undisturbed kinetic flux and total dissipation in the reference area are also shown.

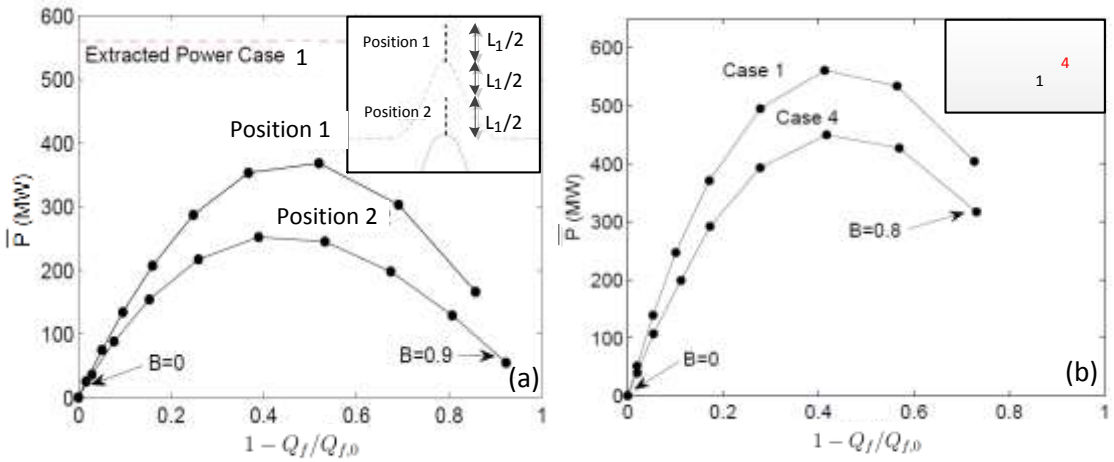


**Figure 7:** Power extraction, plotted against $Q_f$, normalised by the maximum flow rate in the natural state $Q_{f,0}$, for (a) various fence positions in Case 1, and (b) various geometries defined by Cases 1 and 4.

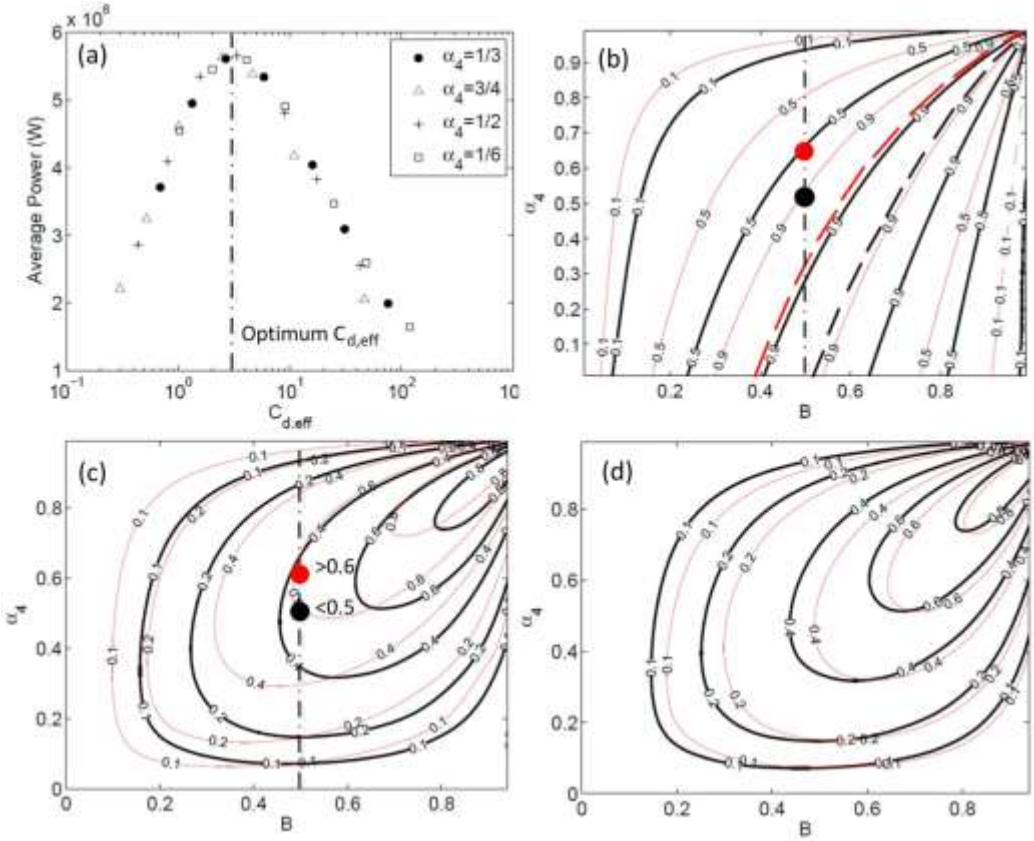


**Figure 8:** (a) extracted power for Case 1. Markers represents blockage ratios taking the values, from left to right: (0.4,0.5,0.6,0.7,0.8,0.85,0.9). The $C_{\mathrm{d,eff}}$ resulting in maximum extraction is labelled, (b) extracted power, normalised by max. extracted power, for Case 1 (thick dark lines) and Case 3 (thin red lines), (c) as in (b) but available power, normalised by max. extractable power, (d) fraction of extracted power, per m of fence, available at two locations along the fence for Case 1: one-fifth of fence length from southern end (thick dark lines), and from northern end (thin red lines). Circles in (b) and (c) indicate max. available power for $B = 0.5$.

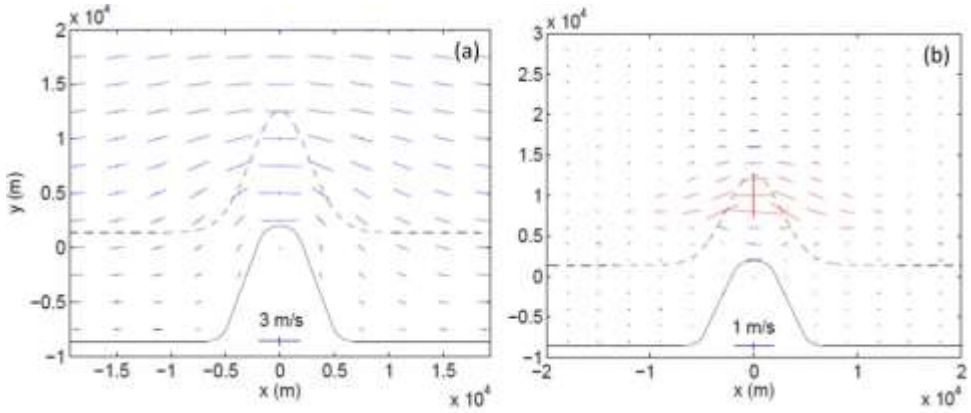


**Figure 9:** Major and minor axes of the M2 velocity ellipse for case 1. (a) Without energy extraction, (b) Absolute difference between natural flow ellipse and those at maximum power extraction. Red (blue) ellipse axes indicate the natural magnitude is higher (lower) than with extraction. The change in ellipse orientation is multiplied by a factor of 3 to make the difference more visible.

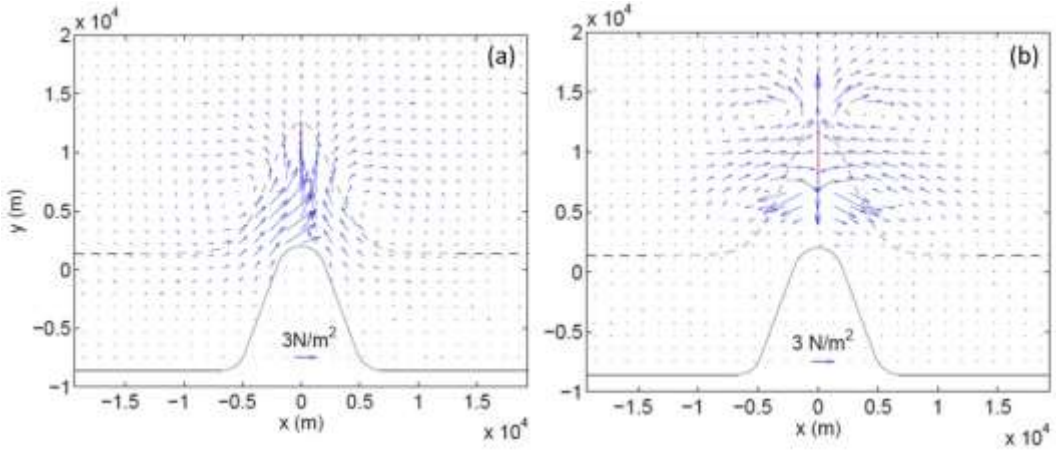


**Figure 10:** (a) Vectors of mean bed shear stress for Case 1 without energy extraction, (b) vector difference in mean bed shear stress for a fence operating at maximum extraction and natural conditions for Case 1.

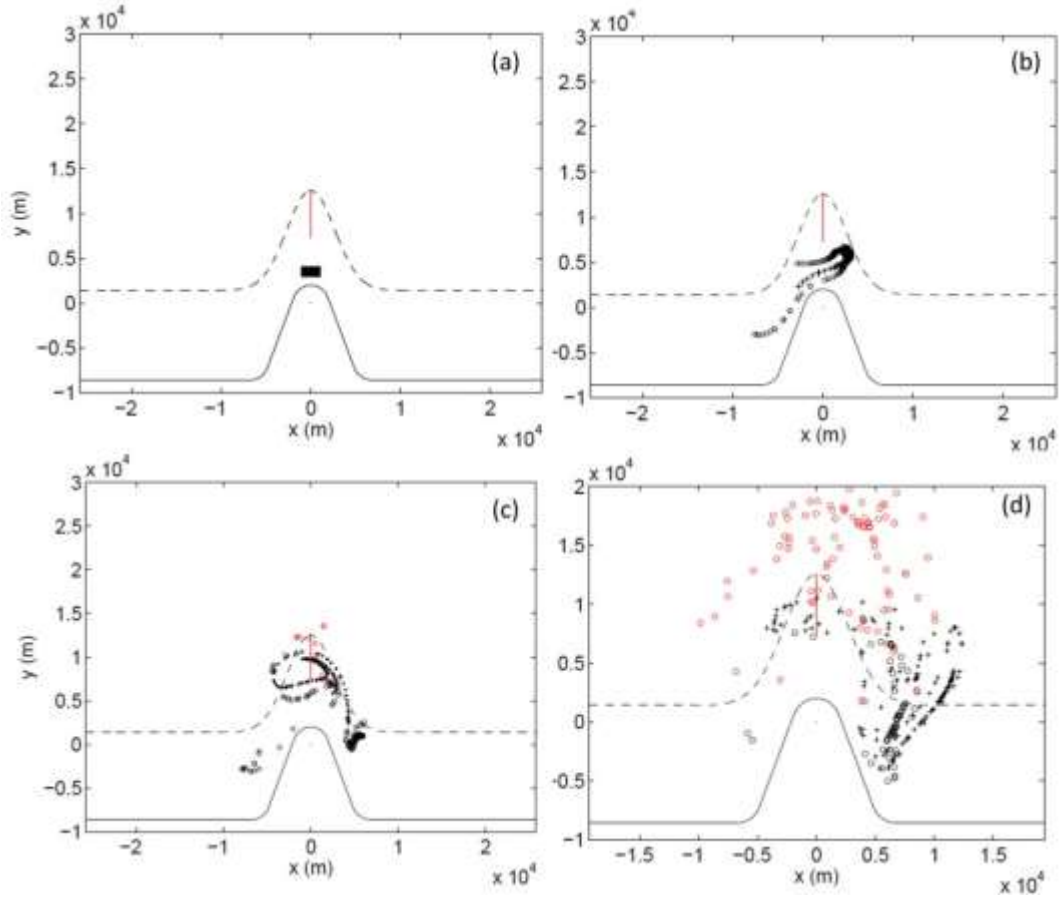


**Figure 11:** Snapshots of particle dispersion released from between the fence and coastline for Case 1. (a) $t/T = 0$, (b) $t/T = 1$, (c) $t/T = 2$, (d) $t/T = 5$. With maximum energy extraction (o), without extraction (•). Red open circles have passed through the turbine fence.

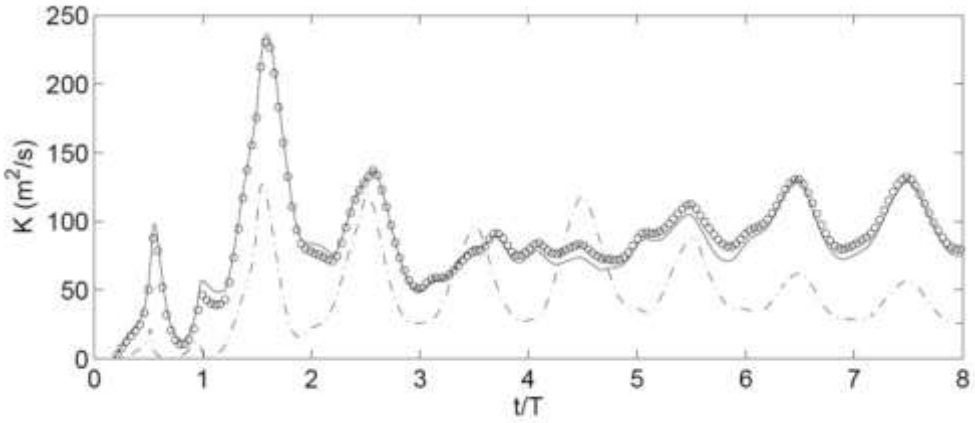


**Figure 12:** Time-varying diffusion coefficient without energy extraction (-.-), at maximum energy extraction (−), and at maximum energy extraction but calculated based on the release of 461 particles (o).